Research Article Vol. 30, No. 5 / 28 Feb 2022 / Optics Express 6746
Optics EXPRESS

Observation of a highly superluminal laser employing optically pumped Raman gain and depletion

ZIFAN ZHOU,[1,*] NICHOLAS CONDON,[2] DEVIN HILEMAN,[2] AND M. S. SHAHRIAR[1,3]

[1]Northwestern University, Department of Electrical and Computer Engineering, Evanston, IL 60208, USA
[2]Digital Optics Technologies, Rolling Meadows, IL 60008, USA
[3]Northwestern University, Department of Physics and Astronomy, Evanston, IL 60208, USA
*zifanzhou2012@u.northwestern.edu

Abstract: In this paper, we report a Raman laser which is extremely sensitive to a variation of the cavity length, using a scheme employing two stable isotopes of Rb. One isotope is used for producing a broad gain spectrum via the optically pumped Raman gain process, while the other is used for producing a narrow dip via the optically pumped Raman depletion process. By tuning the frequencies of the two Raman pumps, the center frequencies of the gain and dip can be aligned to the same frequency. This approach allows tuning of the gain and dip parameters independently over a broad range of operating conditions. With such a configuration, we can produce a negative dispersion around the two-photon resonance frequency in the vapor cell, which leads to a group index that is close to zero. By theoretically matching the experimental observations, we can infer that the sensitivity of such laser is enhanced by a factor of more than 2800, which is nearly a factor of three larger than the highest value reported previously using a different approach.

1. Introduction

Recently, it has been shown that the sensitivity of a laser to a change in the cavity length can be enhanced significantly when the gain profile exhibits critically tuned anomalous dispersion [1–10]. Under this condition, the laser becomes superluminal, in the sense that the group velocity of the lasing field far exceeds the vacuum speed of light, without violating causality or special relativity [11]. The enhancement factor, which can be as high as 10^5 for experimentally accessible parameters [1], is found to be inversely proportional to the group index of the gain medium. To achieve such a small group index for the laser, the gain spectrum of the medium has to have a narrow dip on top of a broad background. For our first demonstration of such a superluminal laser, we employed an approach in which the so-called Diode Pumped Alkali Laser (DPAL) process is used to produce the broad gain in a Rb cell loaded with high pressure buffer gas, and a separate Rb cell with optically pumped Raman depletion is used to produce narrow dip, yielding an estimated enhancement factor of ~190 [12]. However, such an approach cannot be used to produce spatially overlapping bi-directional lasing, which is required for applications such as rotation sensing. This is because the DPAL gain mechanism is bi-directional, leading to mode competition between the two counter-propagating lasers. To circumvent this issue, we switched to a scheme where both the broad gain and the narrow dip are produced via Raman gain and Raman depletion, both of which are highly unidirectional for a warm vapor cell. In this scheme, we used optically pumped Raman gain in ^{85}Rb, and self-pump Raman depletion in ^{87}Rb, and observed an estimated enhancement factor of ~1080 [13]. The optically pumped Raman gain process is highly flexible, allowing for a large range of operating parameters such as the Raman pump detuning and the degree of gain. In contrast, the self-pumped Raman depletion process is highly constrained.

#451132 https://doi.org/10.1364/OE.451132
Journal © 2022 Received 15 Dec 2021; revised 31 Jan 2022; accepted 1 Feb 2022; published 15 Feb 2022

Optics EXPRESS

It works only over a narrow range of Raman pump frequencies, and degree of Raman depletion changes when the Raman pump detuning is changed. Here, we present an approach which overcomes these constraints. In this approach, we replace the self-pumped Raman depletion process by an optically pumped Raman depletion process. We present a theoretical model as well as experimental results. Specifically, we use ^{85}Rb for optically pumped Raman gain [14,15], and ^{87}Rb for optically pumped Raman depletion. The added flexibility in tuning the parameters of the dip in the gain profile enables us to achieve conditions that yield a higher degree of sensitivity than what we had demonstrated earlier. Specifically, we report an estimated enhancement in sensitivity of ~2800, which is nearly a factor of three larger than the highest value achieved previously. The rest of this paper is organized as follows. In Section 2, we present the detailed experimental configuration for observing the highly superluminal Raman lasing. In Section 3, the theoretical model we developed for simulating this scheme is described and explained. In Section 4, the experimental data and the corresponding simulation results are presented and discussed. Lastly, we summarize the conclusions in Section 5.

2. Experimental configuration

The energy levels and the frequency configuration of the optical fields employed for realizing the superluminal laser are shown in Fig. 1. On the left panel, in ^{85}Rb, the optical pump A is tuned to be resonant with the $5S_{1/2}$, F = 2 to $5P_{3/2}$ transition, to produce a population difference between the two hyperfine levels in the $5S_{1/2}$ manifold. The Raman pump A is tuned above the resonance of the $5S_{1/2}$, F = 3 to $5P_{1/2}$ transition, with a detuning denoted as Δ_A. Consider now a probe beam which is tuned above the resonance of the $5S_{1/2}$, F = 2 to $5P_{1/2}$ transition, also with a detuning of Δ_A. Due to the ground-state population inversion produced by the optical pump A, a two-photon gain will be experienced by this probe beam. If the frequency of the probe beam is tuned away from this condition, this Raman gain will drop off, with a linewidth dictated by various factors, including the power of the optical pump A and the power of the Raman pump A. If such a medium is placed inside a cavity, without an actual probe beam, and one of the longitudinal modes of the cavity is tuned to experience this Raman gain, exceeding the round-trip loss, a Raman laser field will be produced.

Consider next the parts shown on the right panel for ^{87}Rb. The optical pump B is tuned to be resonant with the $5S_{1/2}$, F = 2 to $5P_{3/2}$ transition. The Raman pump B is tuned below resonance of the $5S_{1/2}$, F = 2 to $5P_{1/2}$ transition, with a detuning denoted as Δ_B. Consider now a situation where the frequency of the Raman laser field, produced by the ^{85}Rb atoms, is detuned below the $5S_{1/2}$, F = 1 to $5P_{1/2}$ transition, also by the amount of Δ_B. Due to the ground-state population inversion produced by the optical pump B, a two-photon depletion will be experienced by the Raman laser. If the frequency of the Raman laser is tuned away from this condition, this Raman depletion will decrease in strength, again with a linewidth dictated by various factors, including the power of the optical pump B and the power of the Raman pump B. In order to align the center frequencies of the Raman gain process in ^{85}Rb and the Raman depletion process in ^{87}Rb, the values of Δ_A and Δ_B need to be constrained by the relation $|\Delta_A| + |\Delta_B| = 2.28GHz$, which is the frequency difference between the $5S_{1/2}$, F = 2 to $5P_{1/2}$ transition in ^{85}Rb and the $5S_{1/2}$, F = 1 to $5P_{1/2}$ transition in ^{87}Rb. In the experiment, we utilize an offset-phase lock servo (OPLS) to lock the frequency of Raman pump B to that of Raman pump A, with a certain frequency difference between them. Specifically, we first acquire a beat-signal between Raman pump A (with a frequency of f_A) and Raman pump B (with a frequency of f_B). The beat-signal has a sinusoidal component at a frequency of $|f_A - f_B|$. This beat-signal is sent to one of the input ports of the OPLS. In addition, the output of a voltage controlled oscillator (VCO) is sent to another port of the OPLS. The output of the OPLS is fed back to the current controller of Raman pump B, which in turn controls the frequency thereof. When the OPLS is operational, it ensures that the frequency of the VCO matches the beat frequency of $|f_A - f_B|$. Thus, by varying the frequency

Optics EXPRESS

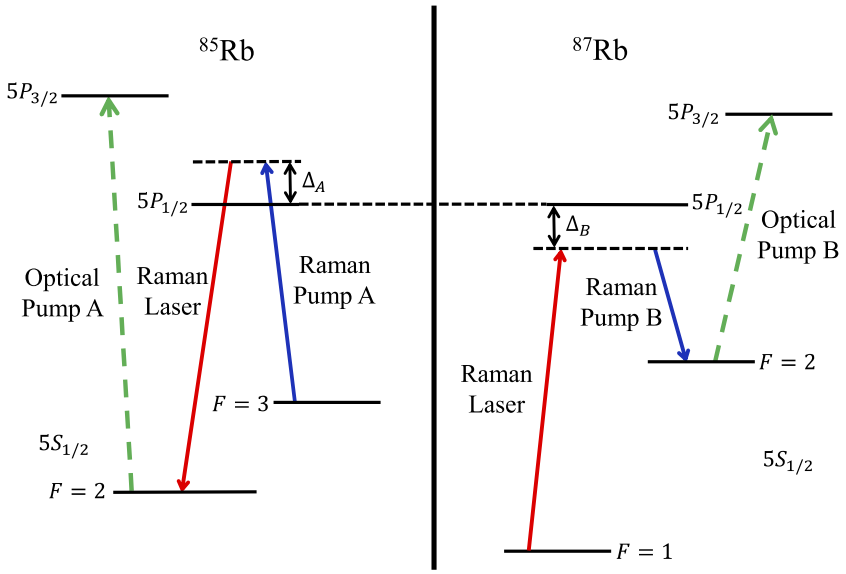

Fig. 1. Relevant energy levels and optical fields in the Rb vapor cell, for ^{85}Rb (left) and ^{87}Rb (right).

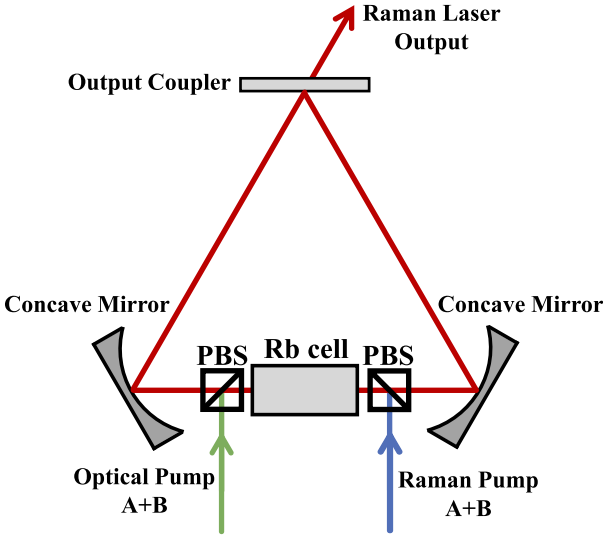

Fig. 2. Schematic illustration of the experimental configuration of the superluminal Raman laser.

of the VCO, we can produce any desired value of $|f_A - f_B|$. In this case, the desired value of $|f_A - f_B|$ is 3.799 GHz.

The schematic of the experimental configuration is shown in Fig. 2. The laser cavity is composed of three mirrors. Each of the two curved perfect reflecting mirrors has the same radius of curvature of 200 mm. The output coupler is a plane mirror with an intensity reflectance of 91.4%. The total cavity length is 226.7 mm. The Rb vapor cell contains the natural mixture with 72.17% of ^{85}Rb and 27.83% of ^{87}Rb. It is heated using bifilarly winded wires. The length of the cell is 50 mm. Due to the fact that the optically pumped Raman gain is maximized when the

Optics EXPRESS

Raman laser field and the Raman pump fields (A and B) are orthogonally polarized, the Raman pumps are coupled into the cavity using a polarizing beam splitter (PBS). After a single pass through the Rb cell, the Raman pumps are coupled out of the cavity through another PBS. The Raman laser beam is produced in the same direction as the Raman pumps since the Raman gain is highly unidirectional. Similarly, we send the two optical pump beams (A and B) into the cavity through the same pair of PBS's, but counter-propagating with the Raman laser as well as the Raman pumps. All the pump beams are focused to a beam-waist diameter that is somewhat larger, by about a factor of 2, than the calculated diameter (~434 μm) of the cavity mode.

3. Theoretical modeling

To match the experimental data, we first establish a theoretical model for the superluminal Raman laser employing this excitation scheme. We make use of a semi-classical model where the atoms are treated quantum mechanically while the optical fields are treated classically. Here we consider an approximate 4-level model for both isotopes. The schematic of the related energy levels and the optical fields employed in the model is shown in Fig. 3(a). In both isotopes, the hyperfine levels in $5S_{1/2}$ are modeled as two different energy levels $|1\rangle$ and $|2\rangle$. Similarly, the hyperfine levels in $5P_{1/2}$ manifold are modeled as $|3\rangle$ and $|4\rangle$. In both isotopes, the Raman laser field is modeled as a probe field, with a Rabi frequency of Ω_s, that couples $|1\rangle \leftrightarrow |3\rangle$ and $|1\rangle \leftrightarrow |4\rangle$ transitions in each isotope. We define the detuning of the Raman laser field as δ_s, with respect to the $|1\rangle \leftrightarrow |3\rangle$ transition in ^{85}Rb. With this definition, the detuning of the Raman laser field with respect to the $|1\rangle \leftrightarrow |4\rangle$ transition can be written as $\delta_s - \omega_1$, with ω_1 being the frequency difference between states $|3\rangle$ and $|4\rangle$ in ^{85}Rb. The detuning of the Raman laser field in ^{87}Rb with respect to the $|1\rangle \leftrightarrow |3\rangle$ transition can then be determined to be $\delta_s' = \delta_s - \omega_2$, with ω_2 being the frequency difference between the $5S_{1/2}$, F = 2 to $5P_{1/2}$, F = 2 transition in ^{85}Rb and the $5S_{1/2}$, F = 1 to $5P_{1/2}$, F = 1 transition in ^{87}Rb. Similarly, the detuning of the Raman laser field with respect to the $|1\rangle \rightarrow |4\rangle$ transition can be written as $\delta_s' - \omega_3$, with ω_3 being the frequency difference between states $|3\rangle$ and $|4\rangle$ in ^{87}Rb. The Raman pump A is tuned above the resonance of the $|2\rangle \leftrightarrow |3\rangle$ transition in ^{85}Rb with a Rabi frequency of Ω_{RPA} and a detuning of Δ_A. The Raman pump B is tuned below the resonance of the $|2\rangle \leftrightarrow |3\rangle$ transition in ^{87}Rb with a Rabi frequency of Ω_{RPB} and a detuning of Δ_B. The Raman pumps also couple the $|2\rangle \leftrightarrow |3\rangle$ and the $|2\rangle \leftrightarrow |4\rangle$ transitions in both isotopes.

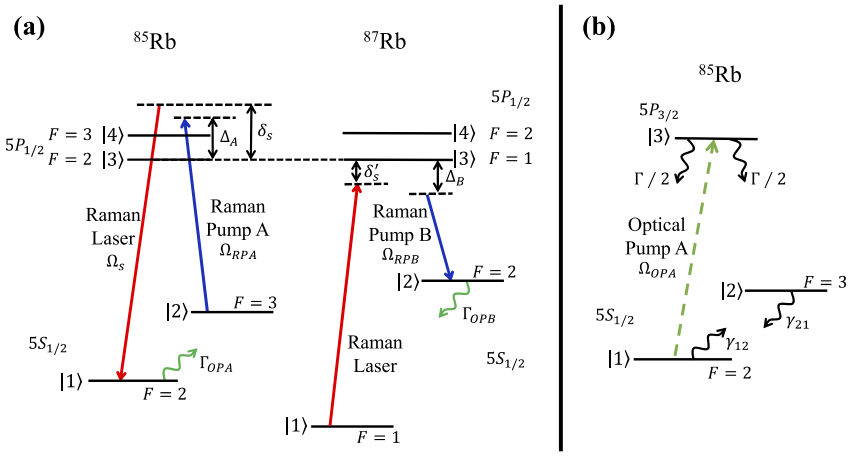

Fig. 3. (a)Related energy levels and optical fields in 4-level models for both Rb isotopes and (b) 3-level system used for calculating effective decay rates accounting for the optical pumping for ^{85}Rb.

Optics EXPRESS

It should be noted that the optical pumping processes are fully incoherent with respect to the Raman pumps and the Raman laser and the optical pump is applied resonantly with respect to the center of the Doppler profile. Thus, if the effect of the optical pump is taken into account explicitly, the light shifts from the atoms above resonance counter-balance the corresponding shifts from the atoms below resonance. As such, there would be no net light shift. Furthermore, the Rabi frequency of the optical pump is significantly smaller than the Doppler width of the transition. Under this condition, the Autler-Townes (AT) type splitting would not occur. Alternatively, it can be stated that the AT-type splitting for atoms within distinct velocity groups would get washed out by the Doppler broadening. Indeed, in another recent paper [16], we have shown experimentally that when the Rabi frequency of the optical pump is increased significantly to be larger than the Doppler width, the effect of Autler-Townes type splitting can be seen, and this effect offers another approach for realizing a superluminal laser. Because of these reasons, the use of an effective decay rate is justified for a four-level model of the system in each isotope. The values of the effective decay rates induced by the two optical pumps are calculated using an effective three-level system for each isotope. This system use for the case of ^{85}Rb is shown in Fig. 3(b), and a similar model is used for the case of ^{87}Rb. Due to the Doppler effect, the spectral absorption width at room temperature is broadened to ~600 MHz, which is significantly larger than the spectral splittings among the hyperfine levels within the $5P_{3/2}$ manifold. As such, this manifold is considered as a single energy level. The natural decay rates from $|3\rangle$ to $|1\rangle$ and $|2\rangle$ are approximated to be equal. The collisional decay rates between the two ground states are also assumed to be equal. Due to the differences in the optical pump configurations, the directions of the effective decay rates are different for the two isotopes, which are denoted as Γ_{OPA} and Γ_{OPB} in Fig. 3(a).

In order to employ a more comprehensive model, it is necessary to take into account the hyperfine levels within the $5P_{3/2}$ manifold, as well as the Zeeman sublevels within each hyperfine level in all three manifolds ($5S_{1/2}$, $5P_{1/2}$ and $5P_{3/2}$) for both isotopes. Such a model would allow for different dipole transition rates among the Zeeman sublevels for a given choice of polarization for each optical field, and assignment of proper branching ratios of decay rates to various Zeeman sublevels in the ground state. We have developed the equations of motion under such a model, based on the N-level algorithm develop earlier by our group [17]. However, the computation time needed, when velocity averaging is carried out, is exorbitantly large, especially for modeling the laser dynamics. Work is underway to optimize the computational codes needed for running such simulations using a supercomputer, and the results would be reported shortly.

To calculate the gain and the dispersion experienced by the Raman laser field, we solve the Liouville equation to find the density matrix in steady state:

$$\frac{\partial}{\partial t}\tilde{\rho} = -\frac{i}{\hbar}(\tilde{\tilde{H}}\tilde{\rho} - \tilde{\rho}\tilde{\tilde{H}}^{\dagger}) + \left(\frac{\partial\tilde{\rho}}{\partial t}\right)_{source}, \tag{1}$$

where $\tilde{\rho}$ is the density matrix in the rotating wave basis, $\tilde{\tilde{H}}$ is the modified Hamiltonian under rotating wave approximations (RWA) and rotating wave transformation, augmented by adding complex terms to diagonal elements in order to represent decay rates of atomic levels, and $(\partial\tilde{\rho}/\partial t)_{source}$ represents the influx of atoms into a state due to decay from another state. The modified Hamiltonian for the 4-level systems in Fig. 3(a) can be written as:

$$\tilde{\tilde{H}}_{85} = \frac{\hbar}{2}\begin{bmatrix} -i(\gamma_{12}+\Gamma_{OPA}) & 0 & \Omega_s & \Omega_s \\ 0 & -2(\delta_s-\Delta_A)-i\gamma_{21} & \Omega_{RPA} & \Omega_{RPA} \\ \Omega_s & \Omega_{RPA} & -2\delta_s - i\Gamma & 0 \\ \Omega_s & \Omega_{RPA} & 0 & -2(\delta_s-\omega_1)-i\Gamma \end{bmatrix}, \tag{2}$$

Optics EXPRESS

$$\tilde{\tilde{H}}_{87} = \frac{\hbar}{2}\begin{bmatrix} -i\gamma_{12} & 0 & \Omega_s & \Omega_s \\ 0 & -2(\delta'_s - \Delta_B) - i(\gamma_{21} + \Gamma_{OPB}) & \Omega_{RPB} & \Omega_{RPB} \\ \Omega_s & \Omega_{RPB} & -2\delta'_s - i\Gamma & 0 \\ \Omega_s & \Omega_{RPB} & 0 & -2(\delta'_s - \omega_3) - i\Gamma \end{bmatrix}, \quad (3)$$

where γ_{12} and γ_{21} are the collisional decay rates between the two ground states, and Γ is the natural decay rates from states $|3\rangle$ and $|4\rangle$ to states $|1\rangle$ and $|2\rangle$. For simplicity, we approximately consider all of these decay rates to be equal. Similarly, the coupling strengths of the $|1\rangle \leftrightarrow |3\rangle$ and the $|1\rangle \leftrightarrow |4\rangle$ ($|2\rangle \leftrightarrow |3\rangle$ and $|2\rangle \leftrightarrow |4\rangle$) transitions are assumed to be equal. As stated earlier, work is underway for developing a more comprehensive model employing all Zeeman sublevels.

The rate of influx of atoms after decaying from the excited states into the ground states for ^{85}Rb and ^{87}Rb are assumed to be the same. These source terms are accounted for as follows:

$$\left(\frac{\partial\rho}{\partial t}\right)_{source-85} = \left[\gamma_{21}\tilde{\rho}_{22} + \frac{\Gamma}{2}(\tilde{\rho}_{33} + \tilde{\rho}_{44})\right]|1\rangle\langle 1| + \left[(\gamma_{12} + \Gamma_{OPA})\tilde{\rho}_{11} + \frac{\Gamma}{2}(\tilde{\rho}_{33} + \tilde{\rho}_{44})\right]|2\rangle\langle 2|. \quad (4)$$

$$\left(\frac{\partial\rho}{\partial t}\right)_{source-87} = \left[(\gamma_{21} + \Gamma_{OPB})\tilde{\rho}_{22} + \frac{\Gamma}{2}(\tilde{\rho}_{33} + \tilde{\rho}_{44})\right]|1\rangle\langle 1| + \left[\gamma_{12}\tilde{\rho}_{11} + \frac{\Gamma}{2}(\tilde{\rho}_{33} + \tilde{\rho}_{44})\right]|2\rangle\langle 2|. \quad (5)$$

We solve the Liouville equations [16] for both isotopes in steady state. After finding the density matrices of the two isotopes in steady state separately, susceptibilities of the two media can be calculated using the expression:

$$\chi_i = \frac{\hbar c n_i \Gamma^2}{2 I_{sat}\Omega_s}(\tilde{\rho}_{31} + \tilde{\rho}_{41})_i, \quad (6)$$

where the subscript i indicates each of the two isotopes (85 and 87), n_i is the number density of the atoms for the i-th isotope, I_{sat} (assumed to be the same for both isotopes) is the saturation intensity which corresponds to a field that produces $\Omega = \Gamma/\sqrt{2}$, and Ω_s is the Rabi frequency of the probe beam, again assumed to be the same for both isotopes. We assume the saturation intensity to be twice as big as that for the strongest transition in the D2 manifold. For a naturally occurring mixture of ^{85}Rb and ^{87}Rb, we make use of the fact that $n_{85} = 0.7217n$ and $n_{87} = 0.2783n$, where n is overall number density of atoms. The overall effective susceptibility of the vapor cell inside the cavity can be expressed as:

$$\chi_{eff} = \frac{L_c}{L}(\chi_{85} + \chi_{87}), \quad (7)$$

where, L is the length of the cavity and L_c is the length of the vapor cell. A typical effective gain spectrum and the corresponding effective dispersion spectrum of the vapor cell are shown in Fig. 4. The parameters used for generating this figure are as follows: the Rabi frequency of the probe beam is $\Omega_{probe} = 0.001\Gamma$, $\Omega_{RPA} = 13.94\Gamma$, $\Omega_{RPB} = 12.06\Gamma$, $\Gamma_{OPA} = 0.3\Gamma$, $\Gamma_{OPB} = 0.02\Gamma$, Γ=2π×6 MHz, and the temperature of the Rb cell is 90°C.

We make use of the semi-classical equation of motion for a single mode laser to analyze the behavior of the system laser under lasing conditions [18]. The real and imaginary parts of χ_{eff} must satisfy the following equations:

$$\omega_s + \dot{\phi} = \omega_{cav} - \frac{\chi'_{eff}}{2}\omega_s, \quad (8)$$

$$\dot{E} = -\frac{\omega_s E}{2Q_{cav}} - \frac{\chi''_{eff}}{2}E\omega_s, \quad (9)$$

where ω_s is the frequency of the Raman laser; ϕ and E are the phase and the amplitude of the Raman laser field, respectively; ω_{cav} is the resonance frequency of the cavity without any medium,

Optics EXPRESS

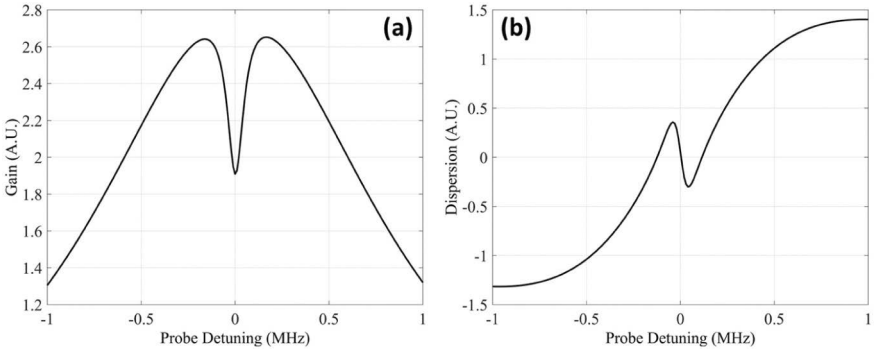

Fig. 4. (a)Typical effective gain spectrum and (b) effective dispersion spectrum experienced by the Raman probe field in the Rb vapor cell before lasing. The parameters used for generating these results are as follows: the Rabi frequency of the probe beam is $\Omega_{probe} = 0.001\Gamma$, $\Omega_{RPA} = 13.94\Gamma$, $\Omega_{RPB} = 12.06\Gamma$, $\Gamma_{OPA} = 0.3\Gamma$, $\Gamma_{OPB} = 0.02\Gamma$, $\Gamma = 2\pi\times 6$ MHz, and the temperature of the Rb cell is 90°C.

which is given by $2\pi mc/L$ with m being the longitudinal mode number; Q_{cav} is the quality factor of the empty cavity; χ'_{eff} and χ''_{eff} are the real and imaginary parts of the susceptibility of the vapor cell, respectively. We adopt an iterative algorithm to find the frequency ω_s and intensity of the laser field in steady state [19], where $\dot{\phi}$ and $\dot{E}$ in Eq. (8) and Eq. (9) are set to zero. The frequency and the intensity of the field can be related with δ_s and Ω_s using the following equations:

$$\omega_s = \omega_0 + \delta_s, \tag{10}$$

$$I_s = 2I_{sat}\left(\frac{\Omega_s}{\Gamma}\right)^2, \tag{11}$$

where ω_0 is the resonance frequency of the $|1\rangle \leftrightarrow |3\rangle$ transition. To explore the relationship between the lasing frequency and cavity length variation, we solve Eq. (8) and Eq. (9) to find the lasing frequency in steady state for different cavity lengths. Here, we define the spectral sensitivity of a laser to be $S \equiv d\omega/dL$, where $d\omega$ is the frequency shift caused by a change in cavity length dL. The sensitivity enhancement factor (SEF) of the Raman laser can be defined as:

$$SEF \equiv \frac{S_{RL}}{S_0}, \tag{12}$$

where $S_0 = -2\pi mc/L^2$, which is the sensitivity of an empty cavity with the same length as the Raman laser, and S_{RL} is the sensitivity of the Raman laser.

4. Results

In Fig. 5(a), we show the experimental data and the corresponding simulation result of the output power of the Raman laser while scanning the frequency of the Raman pump B around two-photon resonance. Experimentally, we fixed the frequency of the Raman pump A to $\Delta_A \simeq 1.36GHz$ and scanned the frequency of the Raman pump B below resonance around $\Delta_{B0} = |\Delta_A - 2.28GHz| = 0.92GHz$. Thus, the horizontal axis in Fig. 5(a) is the deviation of the detuning of Raman pump B away from this value, namely $|\Delta_B| - \Delta_{B0}$. The blue trace in Fig. 5(a) represents the experimental observation. As can be seen, there is a sharp dip in the output power when the magnitude of Δ_B matches the value of Δ_{B0}, as expected. Of course, this reduction in the output power results from the corresponding dip in the gain profile. We have used the numerical model described above to simulate the expected output power, for the experimental

Optics EXPRESS

parameters used: powers of 432 mW and 160 mW for the optical pump A and B, respectively, and powers of 4.2 mW and 4.6 mW for the Raman pump A and B, respectively. The approximate temperature of the cell was 90°C, and the approximate diameter of each of the four beams was 500 μm at the focused spot. As fitting parameters, we varied the temperature slightly around this nominal value, and adjusted the focused spot diameter of each of the four pumps. The best fit, as shown in the red trace in Fig. 5(a), were obtained for a temperature of ~86.8°C, and the focused beam diameters of ~829 μm, ~704 μm, ~643 μm and ~777 μm, for optical pump A, optical pump B, Raman pump A and Raman pump B, respectively, since these parameters are difficult to determine experimentally with high precision. As can be seen, the agreement is remarkably good, with only minor variations of these parameters from their nominal values.

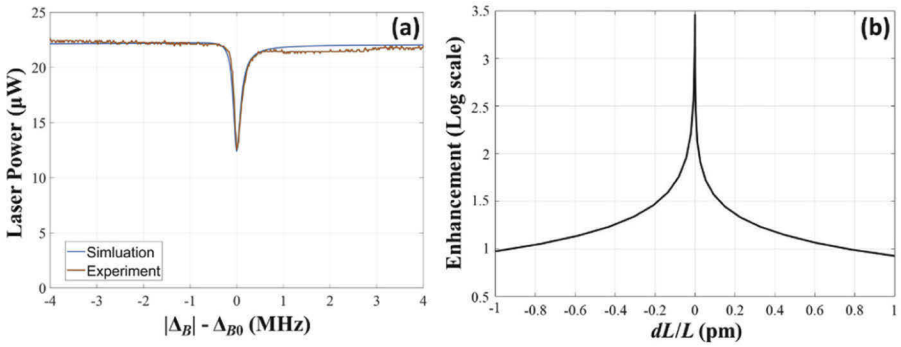

Fig. 5. (a) The experimental data and the simulation result of the Raman laser output power as functions of the deviation of the detuning of Raman pump B away from Δ_{B0} and (b) the calculated SEF of the Raman laser operating at the center frequency of the Raman depletion in Fig. 5(a).

Determining the value of the sensitivity enhancement factor (SEF) experimentally is very difficult for our current experimental setup, since it would require extreme stability against various sources of fluctuations. Efforts are currently underway to build a robust version of this apparatus, mounted on an invar plate, and encased inside a vacuum chamber. In the meantime, we have used the theoretical model to infer the expected value of the SEF. For this process, we choose the operation frequency of the Raman laser as well as the Raman pump B where the SEF is maximized, which is at the center of the depletion shown in Fig. 5(a). The SEF at this operating point is then calculated as a function of the cavity length change. The resulting SEF as a function of the fractional change in the cavity length is shown in Fig. 5(b). As can be seen, the inferred SEF of the Raman laser reaches more than 2800. This is the highest value of the inferred SEF for an experimentally realized superluminal laser so far.

5. Conclusions

In this paper, we experimentally demonstrate a Raman laser which is extremely sensitive to the variation of the cavity length. In this laser, we make use of the two stable isotopes of Rubidium to produce broad gain and narrow dip in the same vapor cell. Specifically, ^{85}Rb is configured to produce a broad Raman gain in a lambda-type 4-level system, and ^{87}Rb is configured to produce a narrow Raman depletion in another lambda-type 4-level system. By tuning the frequencies of the two Raman pumps, the center frequencies of the gain and the depletion can be aligned to the same frequency. With such a configuration, we can produce a negative dispersion around that frequency in the vapor cell, which leads to a group index that is close to zero. The sensitivity of such a laser is enhanced by a factor given by the inverse of the group index. By fitting our experimental results to a numerical model, we infer the sensitivity enhancement factor to be ~

Optics EXPRESS

2800, which is nearly a factor of three larger than the highest value achieved previously using a different scheme.

Funding. Defense Security Cooperation Agency (PO4441028735); Air Force Research Laboratory (FA8649-21-P0959); Air Force Office of Scientific Research (FA9550-18-01-0401, FA9550-21-C-0003).

Disclosures. The authors declare no conflicts of interests.

Data availability. Data underlying the results presented in this paper are not publicly available at this time but may be obtained from the authors upon reasonable request.

References

1. H. N. Yum, M. Salit, J. Yablon, K. Salit, Y. Wang, and M. S. Shahriar, "Superluminal ring laser for hypersensitive sensing," Opt. Express **18**(17), 17658–17665 (2010).
2. M.S. Shahriar, G.S. Pati, R. Tripathi, V. Gopal, M. Messall, and K. Salit, "Ultrahigh enhancement in absolute and relative rotation sensing using fast and slow light," Phys. Rev. A: At., Mol., Opt. Phys. **75**(5), 053807 (2007).
3. G. S. Pati, M. Salit, K. Salit, and M. S. Shahriar, "Demonstration of displacement-measurement-sensitivity proportional to inverse group index of intra-cavity medium in a ring resonator," Opt. Commun. **281**(19), 4931–4935 (2008).
4. G. S. Pati, M. Salit, K. Salit, and M. S. Shahriar, "Demonstration of a Tunable-Bandwidth White Light Interferometer using Anomalous Dispersion in Atomic Vapor," Phys. Rev. Lett. **99**(13), 133601 (2007).
5. M. S. Shahriar and M. Salit, "Application of fast-light in gravitational wave detection with interferometers and resonators," J. Mod. Opt. **55**(19-20), 3133–3147 (2008).
6. D. D. Smith, H. Chang, L. Arissian, and J. C. Diels, "Dispersion-enhanced laser gyroscope," Phys. Rev. A **78**(5), 053824 (2008).
7. D. D. Smith, K. Myneni, Jamiu A. Odutola, and J. C. Diels, "Enhanced sensitivity of a passive optical cavity by an intracavity dispersive medium," Phys. Rev. A **80**(1), 011809 (2009).
8. D. D. Smith, H. Chang, K. Myneni, and A. T. Rosenberger, "Fast-light enhancement of an optical cavity by polarization mode coupling," Phys. Rev. A **89**(5), 053804 (2014).
9. O. Kotlicki, J. Scheuer, and M. S. Shahriar, "Theoretical study on Brillouin fiber laser sensor based on white light cavity," Opt. Express **20**(27), 28234 (2012).
10. D. D. Smith and M. S. Shahriar, "Fast-light optical gyroscopes," topical review, to appear in J. Opt. (2015).
11. L. J. Wang, A. Kuzmich, and A. Dogariu, "Gain-assisted superluminal light propagation," Nature **406**(6793), 277–279 (2000).
12. J. Yablon, Z. Zhou, M. Zhou, Y. Wang, S. Tseng, and M. S. Shahriar, "Theoretical modeling and experimental demonstration of Raman probe induced spectral dip for realizing a superluminal laser," Opt. Express **24**(24), 27444–27456 (2016).
13. Z. Zhou, M. Zhou, and M. S. Shahriar, "Superluminal Raman laser with enhanced cavity length sensitivity," Opt. Express **27**(21), 29738–29745 (2019).
14. P. Kumar and J. H. Shapiro, "Observation of Raman-shifted oscillation near the sodium D lines," Opt. Lett. **10**(5), 226–228 (1985).
15. M. Poelker and P. Kumar, "Sodium Raman laser: direct measurements of the narrow-band Raman gain," Opt. Lett. **17**(6), 399 (1992).
16. Y. Sternfeld, Z. Zhou, J. Scheuer, and M. S. Shahriar, "Electromagnetically induced transparency in Raman gain for realizing a superluminal ring laser," Opt. Express **29**(2), 1125–1139 (2021).
17. M. S. Shahriar, Y. Wang, S. Krishnamurthy, Y. Tu, G. S. Pati, and S. Tseng, "Evolution of an N -level system via automated vectorization of the Liouville equations and application to optically controlled polarization rotation," J. Mod. Opt. **61**(4), 351–367 (2014).
18. M. O. Scully, M. Sargent, and W. E. Lamb, *Laser Phys.*, Westview Press, Boulder, Colorado, 1974.
19. Z. Zhou, J. Yablon, M. Zhou, Y. Wang, A. Heifetz, and M.S. Shahriar, "Modeling and analysis of an ultra-stable subluminal laser," Opt. Commun. **358**, 6–19 (2016).